# Fragmented High-Energy Heavy-Ion Beams for Electronics Testing

Rubén García Alía, Kacper Bilko, Francesco Cerutti, Andrea Coronetti, Natalia Emriskova, Luigi Esposito, Francesc Salvat Pujol, Andreas Waets, Sylvain Girard, Frédéric Saigné, Marco Durante, Christoph Schuy, and Tim Wagner

***Abstract*— Fragmented heavy-ion beams obtained from the interaction of highly energetic ions with thick targets relative to the ion ranges are proposed to mimic the high-penetration linear energy transfer (LET) spectrum present in space and for electronics testing. Our experimental data characterizing fragmented heavy-ion beams show an excellent level of agreement with the Monte Carlo simulations, serving as an initial proof-of-concept of the proposed single-event effect (SEE) testing approach.**

***Index Terms*— Alternative radiation hardness assurance (RHA), high-energy heavy ions, Monte Carlo simulations, nuclear fragmentation, silicon detector, single-event effects (SEEs).**

## I. Introduction

THROUGHOUT the past decade and a half, single-event effect (SEE) testing with very-high-energy (VHE, 100 MeV/u–5 GeV/u) heavy ions has raised great interest in the radiation effects community. Such interest is, on the one hand, motivated by the predominance of VHE ions in the galactic cosmic-ray (GCR) spectrum. Second, it is driven by the more practical reason of their longer ranges in matter and hence improved penetration capacity in microelectronic structures when compared to lower energy ions of easier experimental access. This second reason is becoming increasingly relevant with the aggressive microelectronics integration, including 3-D and system-in-package structures, for which testing with standard (<20 MeV/u) and even high (20–100 MeV/u) energy ions is very challenging or sometimes even unfeasible. Furthermore, high-penetration VHE ion beams covering large enough surfaces also enable board and box-level testing, as well as high-throughput component-level testing.

In [1], a 1-GeV/u iron beam was used in the NASA Space Radiation Effects Laboratory (NSRL) at the Brookhaven National Laboratory (BNL) [2] to perform 90° tilt irradiation tests on static random access memories (SRAMs) and SRAM-based field-programmable gate arrays (FPGAs), without special die or package preparation. The work showed that such test conditions are more representative of the actual space environment, for instance, in terms of induced multiple cell upset (MCU) by long-range ions impinging the chips at grazing angles. It also highlighted that experimental logistics and cost are significant barriers to execute these kinds of tests on a more regular basis.

In [3], a nickel beam in the 100–1000-MeV/u range was used at SIS-18 in Gesellschaft für Schwerionenforschung (GSI) [4] in Germany to test an SRAM-based monitor in a broad linear energy transfer (LET) range, showing a very good single-event upset (SEU) cross-section agreement with results from lower energy ions in the region above the LET threshold, and important discrepancies below it, attributed to differences in the heavy-ion nuclear reaction behavior. The related dataset was extended to other VHE heavy-ion species in [5].

Buchner et al. [6] introduced an original radiation hardness assurance (RHA) approach based on testing parts at different energies separated by small steps and following the general principle inspired by the medical radiation treatment method known as spread out Bragg peak (SOBP). This was obtained by using degraders of different thicknesses, hence ensuring that the Bragg peak of the ions falls close enough to the sensitive volume, regardless of where it is located within the device.

More recently, VHE and ultrahigh-energy (UHE, 5–150 GeV/u) ion tests were performed in the CERN accelerator complex and compared with heavy-ion results at standard energy facilities [7]. These tests were also used to study the effect of the ionization track structure [8] and fragmentation [9], which are largely specific to highly energetic ions. VHE heavy ions were also used at NSRL in [10] for board-level testing, with active parts placed on both sides of the board.

Manuscript received 15 July 2022; revised 26 August 2022 and 11 September 2022; accepted 13 September 2022. Date of publication 5 October 2022; date of current version 18 April 2023. This work was supported by the European Union's Horizon 2020 Research and Innovation Program under Grant 101008126.

Rubén García Alía, Francesco Cerutti, Natalia Emriskova, Luigi Esposito, and Francesc Salvat Pujol are with CERN, CH-1211 Geneva, Switzerland (e-mail: ruben.garcia.alia@cern.ch).

Kacper Bilko is with CERN, CH-1211 Geneva, Switzerland, and also with Laboratoire Hubert Curien UMR 5516, UJM-Saint-Etienne, University of Lyon, F-42023 Saint-Étienne, France.

Andrea Coronetti is with CERN, CH-1211 Geneva, Switzerland, and also with the Institute d'Électronique et des Systèmes, Université de Montpellier, 34090 Montpellier, France.

Andreas Waets is with CERN, CH-1211 Geneva, Switzerland, and also with the Medical Physics and Radiation Research group, University of Zurich, 8006 Zurich, Switzerland.

Sylvain Girard is with the Laboratoire Hubert Curien UMR 5516, UJM-Saint-Etienne, University of Lyon, F-42023 Saint-Étienne, France.

Frédéric Saigné is with the Institute d'Électronique et des Systèmes, Université de Montpellier, 34090 Montpellier, France.

Marco Durante, Christoph Schuy, and Tim Wagner are with GSI Helmholtzzentrum für Schwerionenforschung, 64291 Darmstadt, Germany.

Color versions of one or more figures in this article are available at https://doi.org/10.1109/TNS.2022.3210403.

Digital Object Identifier 10.1109/TNS.2022.3210403

Monte Carlo simulations of VHE ion energy loss and fragmentation are crucial to complement experimental results and perform SEE rate predictions. In [11], different nuclear physics models are compared in terms of VHE ion fragmentation and related energy deposition. In [12], [13], and [14], Monte Carlo codes were used in combination with experimental data to estimate the nuclear reaction contribution to heavy-ion SEEs in space. Likewise, the effect of delta rays on the deposited energy by UHE ions in relatively large (hundreds of $\mu$m) sensitive volumes is covered both experimentally and through simulation in [15] and [16].

The experimental and simulation studies above have determined that one of the main limitations of VHE ion testing is the tradeoff between the maximum LET attainable and the accuracy of the LET at a sensitive volume level. In other words, the largest LET values are obtained at the end of the range of the particles, over relatively short distances. Hence, if the location of the sensitive volume and overlayer thickness and composition are not accurately known (as is typically the case), there will be a large uncertainty on the LET value at the sensitive location. This problem becomes more pronounced for 3-D or system-on-chip devices which may have multiple sensitive volumes at different depths, as well as for board-level testing, for which devices can, for instance, be placed on different sides of the printed circuit board (PCB) [10]. This limitation can be overcome by using VHE beams for which the LET does not significantly vary over mm or even cm of matter, but this comes at the cost of using absolute LET values that are too low for most qualification purposes.

Therefore, the experimental approach proposed in this work is mainly targeted at overcoming this limitation, by offering a test condition that simultaneously ensures a high LET as well as high penetration with a constant LET profile. As will be explained in Section II, this can be achieved through the nuclear fragmentation of a high-energy heavy-ion beam, exploiting the similarity of the resulting LET spectra with that of GCRs in the space environment.

## II. Concept Introduction: LET Spectra of Fragmented Beams

Degraders such as polyethylene, aluminum, or air are routinely used in facilities accelerating ions up to 100 MeV/u to modify the energy, and hence LET, of the beams used for electronics testing. This technique is especially suited for cases in which the thickness of the degrader is much smaller than the nuclear interaction length of the ions and for which the dominant effect is therefore the energy loss through direct ionization, as opposed to the ion fragmentation.

For larger energies, the degrader thicknesses needed to significantly alter the energy of the beam also become larger, both in absolute terms, as well as relative to the inelastic interaction length, which is fairly constant with energy [8] in the VHE range. This means that, in order to retrieve sufficiently large energy variations, a nonnegligible fraction of the beam has to undergo fragmentation, reducing the intensity of the primary ions, while introducing secondary products.

This effect is depicted in Fig. 1, in which the differential LET(Si) spectrum of a 1-GeV/u lead beam is scored using

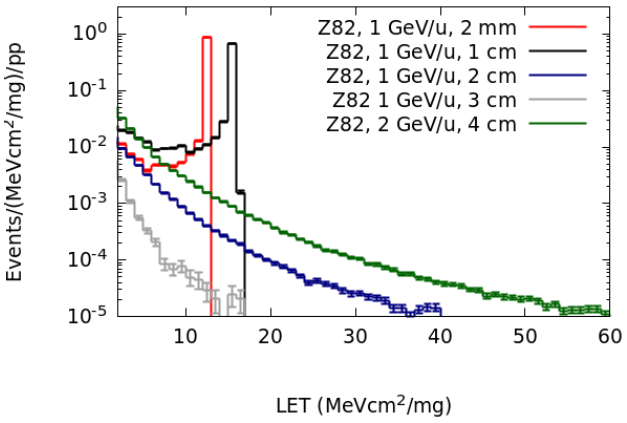


Fig. 1. Differential LET distribution resulting from the interaction of 1- and 2-GeV/u lead ions with different copper thicknesses, plus 3 m of air, as simulated in FLUKA.

the FLUktuierende KAskade (FLUKA) Monte Carlo code [17] (version 4-2.1 by CERN) for different copper thicknesses, and including also 3 m of air between the degrader and scoring region. More details about FLUKA and simulation settings used in this work are included in Section IV. As can be seen, for values up to 1 cm of degrader thickness included, the main effect on the primary ion beam is that of reducing its energy (hence increasing its LET, from the initial value of 11.9 MeVcm$^2$/mg). In addition, the fragmentation level increases with the degrader thickness, resulting in fragments that mostly have lower LETs than the primary ion, given their similar energy per nucleon and lower charge.

As the degrader thickness increases to 2 cm and surpasses the range of the primary beam (17.4 mm in copper), the LET peak corresponding to the primary ions disappears, and only the fragments remain. In this case, the fragments can have much larger LET values than the primary beam due to their energy loss in the target and the air before reaching the scoring region. At 3 cm of copper target thickness, the fragments are less numerous, and with lower LET values. The case of 2-GeV/u Pb ions on a 4-cm copper target is also included for completeness, as it is used later on in this section.

Hence, above a certain thickness, the degrader is acting more as a "fragmenter," and the resulting beam is dominated by fragmentation products.

Moreover, it is possible to compare the fragmented VHE beam LET spectra with that present in the GCR spectrum in space. Fig. 2 shows the integral LET spectrum as extracted using the Cosmic Ray Effects on MicroElectronics (CRÈMEs) online tool [18], with the CREME96 GCR version [19], solar minimum conditions, a near-Earth Interplanetary location, all ions up to $Z = 92$ with energies above 0.1 MeV/u as input, and 100 mils (2.54 mm) of aluminum shielding. The CREME GCR LET spectrum is also shown for the subset of ions with $40 \leq Z \leq 92$, well above the so-called iron knee. In addition, the LET spectra of two fragmented beams are included, for primary energies of 1 and 2 GeV/u, and copper thicknesses of 2 and 4 cm, respectively, and normalized to the GCR fluence above an LET value of 40 MeVcm$^2$/mg. As can be seen,

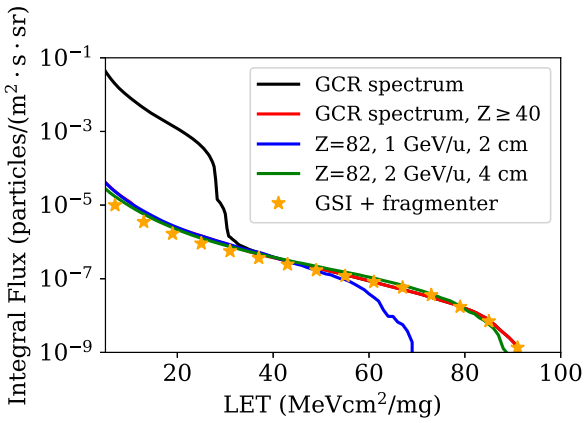


Fig. 2. Reverse integral of the GCR spectrum as extracted from CREME, compared to two fragmented lead beams and the GSI experimental case, consisting of an 800-MeV/u uranium beam on a PMMA fragmenter, as described in Section III, all normalized to the integral flux above 40 MeVcm$^2$/mg.

the former very well reproduces the GCR spectrum up to ∼55 MeVcm$^2$/mg, whereas in the case of the latter, the agreement extends up to ∼85 MeVcm$^2$/mg. It is worth recalling at this stage that the simulated data shown in Fig. 2 corresponds to the same one as Fig. 1, but represented in integral rather than in differential form, and normalized to the GCR high-LET (>40 MeVcm$^2$/mg) ion flux, which corresponds to $6.7 \cdot 10^{-8}$ ions/cm$^2$/s, a value that we will later use to calculate the acceleration factor of the proposed test approach. Moreover, the experimental conditions used at GSI, and covered in Sections III and IV, are also included in Fig. 2, as will be discussed later in this article. However, we already note at this stage that GSI measurements and simulations were performed with uranium on polymethyl methacrylate (PMMA), instead of lead on copper.

Therefore, even if fragmentation can initially be seen as an adverse effect that alters the properties of the primary VHE heavy-ion beams used for testing, it is also one of the effects that gives shape to GCR spectra in space, which, in turn, closely reproduce the related LET spectra if an adequate combination of primary beam and energy, and target material and thickness are selected.

Moreover, as will be shown in more detail in Section IV, the fragmented beams originating from VHE ions can penetrate matter without substantially modifying their intensity and LET spectra. For instance, in the case of 2-GeV/u lead ions on 4 cm of copper, after 5 mm of silicon (note that similar conclusions apply to its neighbor in the periodic table, aluminum, commonly used as shielding in space applications), the intensity reduction is only ∼20% of the original value, and the relative LET spectrum is unperturbed.

It is worth noting at this stage that, although performing heavy-ion SEE tests on electronics with LET spectra is a novel approach with respect to multiple mono-LET irradiations yielding an SEE cross section versus LET, similar approaches are routinely applied when using high-energy proton beams to generate spallation environments for atmospheric [20] or high-energy accelerator [21] applications. Similarly, testing

TABLE I

$^{238}$U BEAM CHARACTERISTICS AS PROVIDED BY THE FACILITY AND MEASURED WITH THE DIODE. THE ENERGY IS GIVEN AT THE VACUUM WINDOW

| | unit | Non-fragmented | Fragmented |
|---|---|---|---|
| PMMA thickness | cm | 0 | 6.2 |
| Energy at beam window | MeV/u | 800 | 800 |
| LET(Si) | MeV cm$^2$/mg | 15 | 0-70 |
| Fluence by the facility | Ions/cm$^2$ | $1.5 \cdot 10^5$ | $5 \cdot 10^5$ |
| Acquisition duration | s | 234 | 1416 |

with a degraded 70-MeV proton spectrum was proposed in [22] in order to determine the low-energy proton sensitivity by obtaining spectra similar to those present in the trapped proton belts in space. Along similar lines, García Alía [13] and Foster [23] proposed a direct comparison between the LET spectrum in space and that generated by high-energy hadron nuclear interactions in silicon. The former was found to match the latter up to an equivalent LET of roughly 10 MeVcm$^2$/mg, hence enabling the prediction of SEE rates for components with low LET thresholds, as is typically the case for soft errors, as well as for screening out parts with very low destructive SEE thresholds.

Likewise, previous and ongoing efforts [24], [25], [26] have focused on reproducing the GCR energy and LET spectra in ground-based facilities; however, these have focused on radiobiology applications and are hence not tailored to nor benchmarked for electronics testing applications.

## III. GSI PROOF OF CONCEPT: EXPERIMENTAL MEASUREMENTS

One of the key challenges for fragmented VHE ion testing is the related beam characterization and dosimetry. As highlighted in [11], measuring the energy deposition spectra of fragmented beams is of great importance, mainly due to the differences that exist among the various Monte Carlo codes and nuclear physics models.

Measurements have been recently performed using solid-state silicon and diamond detectors in VHE and UHE beams [27]. These results revealed a significant presence of fragments, in addition to the primary beam, which corresponds to the prominent peak in the energy deposition distributions.

As part of this work, heavy-ion beam fragmentation measurements were performed with the experimental setup shown in Fig. 3, using 800 MeV/u $^{238}$U ions in the GSI-SIS18 facility in Germany, with a projected range of 39 mm in silicon and an LET(Si) of 15 MeVcm$^2$/mg, as retrieved through SRIM [28]. The beam parameters are listed in Table I.

The core of the setup was a 300-$\mu$m-thick silicon diode (exposed silicon surface: 0.5 cm$^2$) produced by Canberra (model: FD 50-14-300 RM), as shown in Fig. 4. The detector was operated under a reverse bias of 60 V, sufficient for a full silicon depletion. The signal was amplified through the Cividec C1-HV current-sensitive preamplifier (21.9 dB amplification) and further attenuated by 6 dB, resulting in the effective amplification of $g = 15.9$ dB. The data

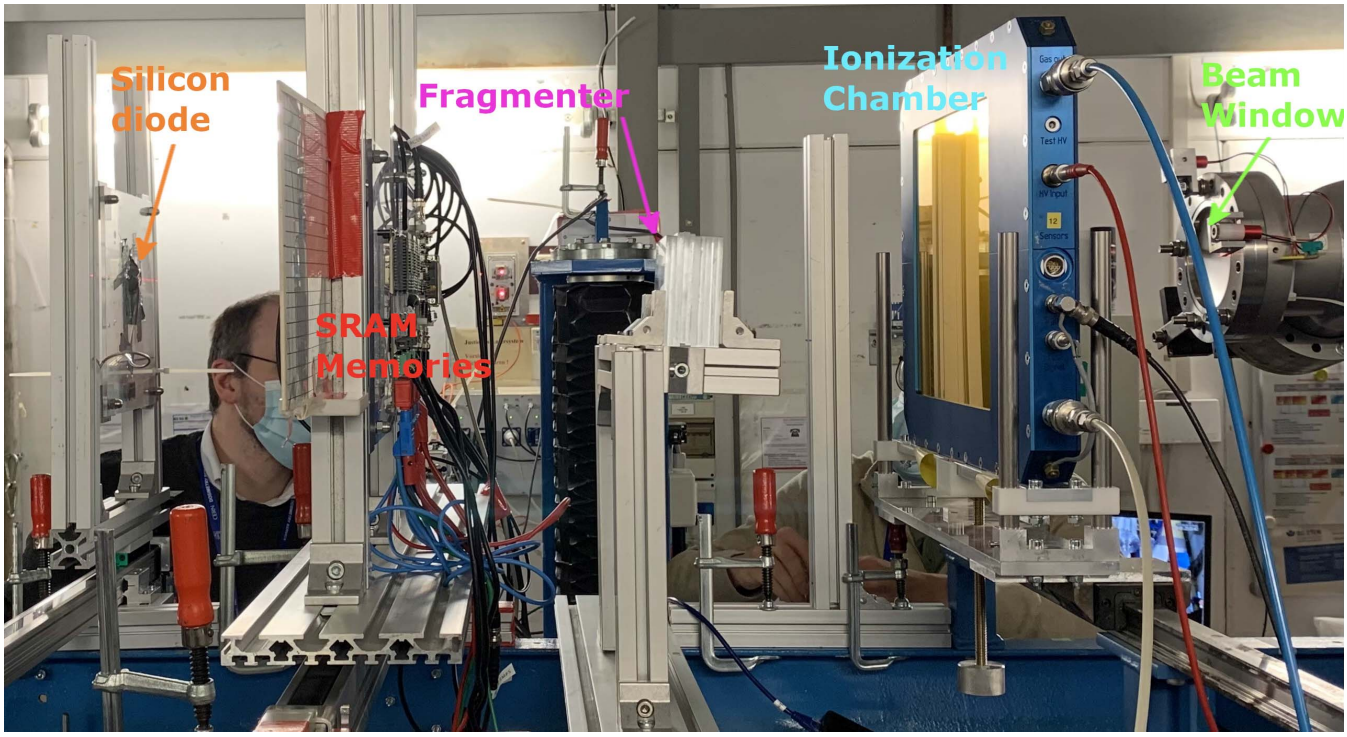


Fig. 3. Experimental setup during $^{238}$U irradiations in the GSI-SIS18. Depending on the acquisition, either the silicon diode or the SRAM memories were exposed to the beam. The fragmenter consisted of several slabs of PMMA with a total thickness of 6.2 cm. During the experimental run with the fragmenter, the silicon diode was 72 cm downstream of the fragmenter, whereas, for all presented acquisitions, the distance between the diode and the beam vacuum window was constant and equal to ∼117 cm.

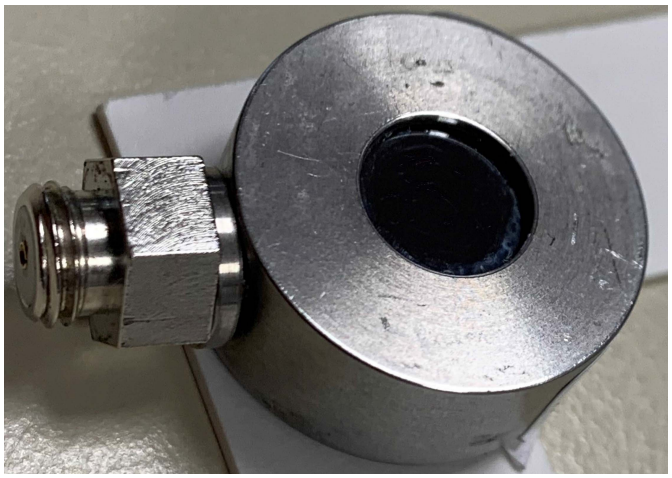

Fig. 4. 300-$\mu$m-thick silicon detector manufactured by Canberra used to measure the energy deposition by the fragmented and nonfragmented beams.

acquisition was performed using the 1-GS/s Caen digitizer (model DT5751).

The deposited energy $E_{\text{dep}}$ of each event was calculated as the integral of the measured diode current $I(t)$ over time [see (1)], with the assumption that on average $k = 3.91$ eV energy is needed to create one electron–hole pair via ionization. The $k$ factor was retrieved through the calibration with the 16.3-MeV/u heavy ions, at the Radiation Effect Facility (RADEF) in Finland [29]

$$E_{\text{dep}} = \frac{k}{g} \int I(t)dt. \tag{1}$$

The resulting energy deposition distributions can be seen in Fig. 5 and will be discussed in more detail in Section IV, in comparison with the Monte Carlo simulation results. However, we can already highlight at this stage the very different qualitative distribution behavior, with the primary beam run showing clearly defined peaks, and the fragmented beam exhibiting a broader distribution, extending also to significantly larger deposited energies.

## IV. GSI Proof of Concept: Monte Carlo Simulations

To understand the physical behavior of VHE ion beams and their interaction with matter, simulations can be used both in the test preparation, but also to verify and extend experimental findings. The stochastic nature of particle interactions and secondary particle production can naturally be described using Monte Carlo-based simulation methods. The general-purpose code FLUKA is regularly used at CERN with proven capability in accelerator design problems, detector studies, dosimetry, radiation protection, medical physics, and space research [17], [30]. It has been subject to systematic testing and extensive benchmarking on a microscopic level, and therefore it is a highly suitable tool to describe the physical interactions

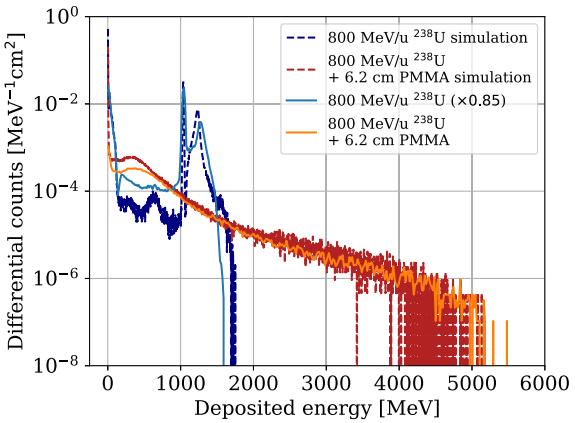


Fig. 5. Energy deposition spectrum from the GSI 800-MeV/u uranium beam measured with the 300-$\mu$m-thick silicon solid-state detector normalized to the delivered fluence (as provided by the facility) and the histogram bin width. Additionally, the simulated energy depositions are depicted, as retrieved via the FLUKA Monte Carlo Code. The measured energy deposition spectrum for the configuration without the PMMA fragmenter has been multiplied by 0.85 horizontally for visualization purposes.

of the beam and deepen the understanding of the measured quantities.

FLUKA allows tuning of the production and transport of particles specifically to the simulation needs. This study, in particular, involved detailed transport of ions including the necessary interaction mechanisms to describe fragmentation processes such as fission, evaporation, coalescence, and electromagnetic dissociation. To account for all possible secondary particles generated through inelastic interactions, the production and transport of hadrons, muons, and neutrinos is enabled down to 1-keV kinetic energy, and for neutrons down to $10^{-5}$ eV. Electrons (including delta rays), positrons, and photons are generated and transported down to 150 keV.

The geometric model shown in Fig. 6 and the beam parameters were implemented in such a way to accurately represent the experimental conditions at GSI. A uniform $^{238}$U beam with a $2 \times 2$ cm$^2$ surface area is generated in a vacuum behind a 50-$\mu$m stainless steel vacuum window. It is propagated in air, passing through a 4-cm-thick ionization chamber filled with $ArCO_2$ gas before impacting the PMMA fragmentation target (using the predefined International Commission on Radiation Units and Measurements, ICRU, compound implemented in FLUKA with a density of 1.19 g/cm$^3$). Note that this target was absent in the nonfragmented beam case. The thickness of the target was set to 62 mm, in order to be slightly thicker than the range of an 800 MeV/u $^{238}$U in PMMA, corresponding to 52 mm, as obtained using SRIM [28]. The silicon diode is located roughly 1 m downstream of the vacuum window, including the 300-$\mu$m-thick sensitive layer embedded within its casing and covered with a 20-$\mu$m aluminum layer. Otherwise, no energy spread was considered for the incoming beam in the simulation (i.e., the beam extracted from the synchrotron) as the energy spread at the location of the DUT is fully dominated by the energy loss in the beamline elements, and is therefore explicitly accounted for in the simulation. As a result of this energy loss, the average beam energy at the DUT location for the 800-MeV/u $^{238}$U ion is calculated to be 786.5 MeV/u, with an FWHM of 0.4 MeV/u.

The primary physical quantity scored is the event-by-event energy deposition within the 300-$\mu$m Si layer shown in Fig. 5. In the nonfragmenter case, the energy deposition peak at roughly 1 GeV corresponds to primary $^{238}$U ions. Several dedicated scorings of particle LET and $Z$ distributions were included to distinguish events in the diode layer caused directly by primary beam particles versus those that are subject to interactions with the diode casing. This allowed us to understand the second, broader energy deposition peak at roughly 1.3 GeV as originating from primary $^{238}$U ions undergoing additional energy loss by traveling through the casing materials before arriving in the diode layer with a larger LET than the primary beam. Similar double-peak structures have been observed and described for the same diode and casing in [15] and [16], however in these cases at significantly larger heavy-ion energies, for which the extra energy deposition by ions traveling through the diode cover is not related to the ion energy loss and increased LET, but rather to the high-energy delta rays generated in it.

These features are fully absent in the PMMA fragmenter case, where only a continuous spectrum of ion fragments up to $Z = 75$ remains. The primary beam is fully fragmented and the energy deposition spectrum of the lower-$Z$ fragments shows events above 4 GeV, by consequence indicating much higher LET values in the silicon diode when compared to the nonfragmented case. The corresponding simulated LET spectrum is shown in Fig. 2 and matches very well the GCR spectrum above 40 MeVcm$^2$/mg. When scored at different depths within the 300-$\mu$m silicon layer, the resulting LET distribution remains unchanged as shown in Fig. 7.

An important figure-of-merit of this approach is the yield of high-LET (>40 MeVcm$^2$/mg) ions generated per unit of primary high-energy heavy-ion beam fluence, as well as the dose. The first value is a ratio between the same physical quantity and is therefore unitless. According to the simulations, the ratio between the high-LET secondary ion fluence and the primary beam fluence is $4.16 \cdot 10^{-5}$. Likewise, the deposited total ionizing dose [TID(Si)] at the device under test (DUT) location per unit primary fluence is equal to $1.62 \cdot 10^{-7}$ Gy $\cdot$ cm$^2$. As will be discussed in Section VI, these values have important implications for the practical implementation of the proposed approach.

In addition, particle fluences were scored to estimate the number of light secondaries such as protons and neutrons generated by the target, both at the target as well as at the diode location as shown in Fig. 8 for neutrons. This allows estimation of the light secondary particle fluences produced by the target in addition to the heavy-ion fragment spectrum, which can impact neighboring test devices or auxiliary electronic equipment in an experimental scenario. Per unit primary fluence, the heavy-ion impacts on the PMMA fragmenter produce a cumulative fluence of $3 \cdot 10^2$ neutrons cm$^{-2}$ with energy above 20 MeV, scored at the downstream end of the fragmenter block as shown in Fig. 6. At the diode location, the neutron fluence above 20 MeV is reduced by a factor of 3. It is to be noted, however, that the simplified FLUKA geometry model

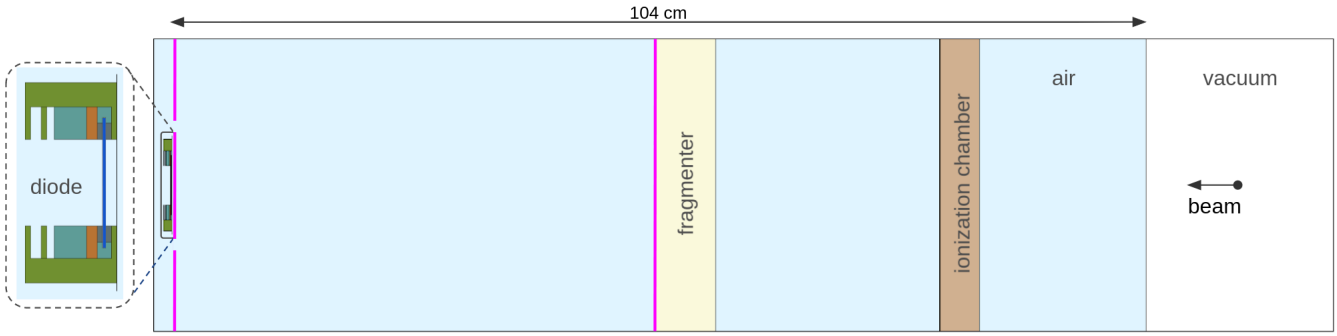


Fig. 6. Schematic of the geometry used in the FLUKA simulations. The dimensions, composition, and density of all materials are implemented such that it accurately represents the test configuration shown in Fig. 3. The simulated volume is restricted to the beam path and its immediate surroundings (1.5-cm radius). The inset on the left shows a detailed view of the diode geometry model, including the 300-$\mu$m silicon layer (in blue) where energy deposition events and particle spectra are scored. In addition, the planes where secondary particle fluences (protons, neutrons) are scored are indicated in pink.

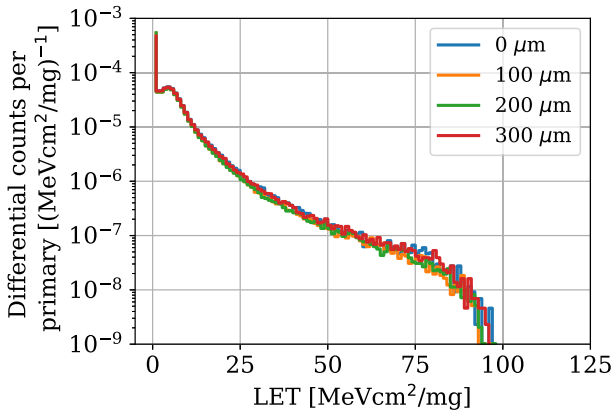


Fig. 7. FLUKA simulation results of LET distribution versus the depth in steps of 100 $\mu$m inside the silicon layer of the diode in the 6.2-cm fragmenter case, normalized per primary simulated particle. Within the full thickness of the silicon layer of 300 $\mu$m, the resulting LET distribution remains unchanged.

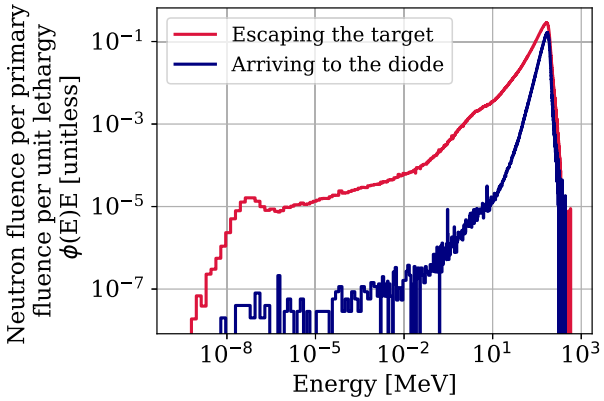


Fig. 8. FLUKA simulation results of the neutron fluence generated by the interaction of the $^{238}$U beam with the PMMA target. Lethargy fluences (i.e., differential fluences times the bin energy) are expressed per simulated beam particle fluence and scored at two different locations: at the downstream edge of the target, and in the surrounding area directly surrounding the diode. Calculating the secondary radiation field in the vicinity of the DUT can help to estimate the SEE risk for auxiliary electronic equipment.

of the beam line does not include its surrounding materials and walls and is therefore not representative of possible neutron scattering and thermalization.

From a computational point of view, it is worth noting that the simulation studies were carried out on a dedicated computing processing unit cluster for FLUKA applications at CERN consisting of a combination of Intel Xeon and AMD Epyc processors as nodes. On average, the amount of simulated primary particles needed to achieve statistically converged results at the diode location was on the order of 800 K without the fragmenter; when the fragmenter was introduced, the number of primaries had to be increased by a factor of 4 to obtain results of the same quality. Simulating high-energy heavy ions is a computationally demanding task due to the required physics processes and amount of secondary particles produced in inelastic interactions, as well as the need of transporting them down to relatively low energies, including electrons, in order to accurately retrieve the energy deposition distributions of interest in relatively small scoring regions. Restricting the simulation volume to the minimum allows completion of the simulation of one primary particle in around 4 s on average, without using any biasing techniques; incorporating the fragmenter increases this average to 8 s.

## V. Radiation Hardness Assurance Applications

The approach presented in Section II and further developed in Sections III and IV can be exploited for RHA purposes. Electronics can be irradiated with a fragmented heavy-ion beam, such as that obtained experimentally at GSI, and the rate of SEEs in space can then be calculated based on the measured event rate or cross section. In order to evaluate the accuracy of such an approach, a set of 82 single-event latchup (SEL) heavy-ion cross-section datasets and related response functions are taken from the recent literature [31], [32], [33], [34], [35], [36], [37], [38], [39], [40], [41], [42], [43], [44], [45], [46], [47], [48], [49].

Two different in-orbit SEL rates are calculated for each of the 82 parts. The first one ($R_{\mathrm{GCR}}$) is obtained by folding the heavy-ion response function [in the Weibull form of (2)] with the GCR spectrum as a function of LET (i.e., standard SEE rate calculation approach, considering, however,

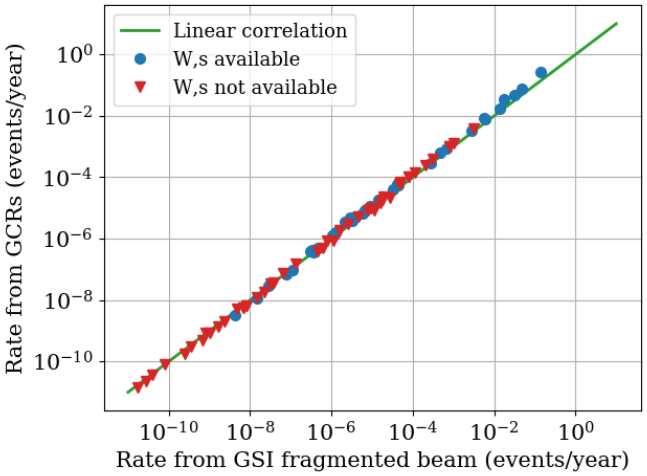


Fig. 9. Calculated space SEL rate for the 82 response functions considered, using GCR spectrum (vertical axis) and fragmented 800-MeV/u $^{238}$U ion spectrum (horizontal axis), scaled with the ratio of the GCR and fragmented fluxes above 40 MeVcm$^2$/mg. In the case of response functions for which $W$ and $s$ are unknown (red markers), the average values of 30 MeVcm$^2$/mg and 3 are considered, respectively.

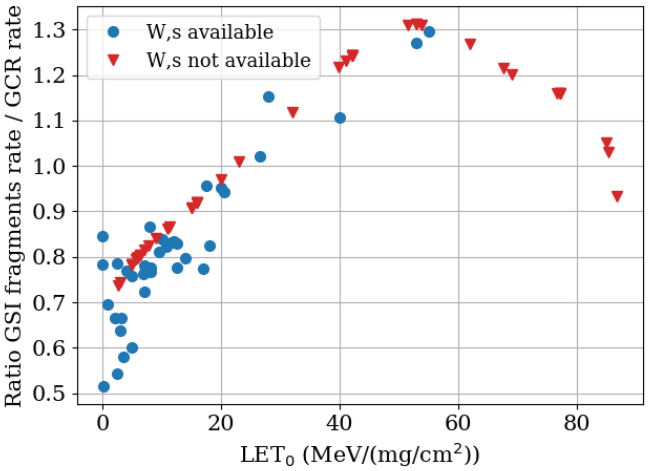


Fig. 10. Ratio between the calculated space SEL rates with the fragmented 800-MeV/u $^{238}$U ion spectrum and that from the GCR spectra for the 82 response functions considered. Results are plotted with respect to the device onset LET.

a mono-directional scenario, as opposed to an isotropic one), in this case only including ions with $Z \geq 40$, that is, $\Phi_{Z\geq 40}(\text{LET})$, and as per (3).

The second one ($R_{\text{GSI}}$) consists in folding the heavy-ion response function with the ion spectra obtained at GSI upon fragmentation of the 800-MeV/u $^{238}$U beam and scaled with the ratio between the space, $\Phi_{Z\geq 40}(\text{LET})$, and experimental, $\Phi_{\text{exp}}(\text{LET})$, ion fluences above 40 MeVcm$^2$/mg, and as per (4). In this equation, $R_{\text{exp}}$ would typically correspond to the SEE rate retrieved experimentally using the fragmented heavy-ion beam and in the scope of this work is calculated as per (5).

In terms of response functions, the literature dataset is not fully homogeneous, that is, in some cases, only the saturation cross-section $\sigma_{\text{sat}}$ and onset LET (LET$_0$) are known, but not the Weibull shape parameter $W$ and exponent $s$. When the latter is not available, for a first calculation, average values of 30 MeVcm$^2$/mg and 3 are respectively considered based on the data from the devices for which these parameters were available

$$\sigma(\text{LET}) = \sigma_{\text{sat}} \cdot \left(1 - \exp(-(\text{LET} - \text{LET}_0)/W)^s\right) \quad (2)$$

$$R_{\text{GCR}} = \int \Phi_{Z\geq 40}(\text{LET}) \cdot \sigma(\text{LET}) \cdot \text{dLET} \quad (3)$$

$$R_{\text{GSI}} = R_{\text{exp}} \cdot \frac{\int_{40}^{\infty} \Phi_{Z\geq 40}(\text{LET}) \cdot \text{dLET}}{\int_{40}^{\infty} \Phi_{\text{exp}}(\text{LET}) \cdot \text{dLET}} \quad (4)$$

$$R_{\text{exp}} = \int \Phi_{\text{exp}}(\text{LET}) \cdot \sigma(\text{LET}) \cdot \text{dLET}. \quad (5)$$

Fig. 9 provides a direct comparison between the two SEL rates for all the considered devices. Indeed, by scaling the fragmented beam SEE rate with the ratio of fluences above 40 MeVcm$^2$/mg, the level of agreement is excellent for all the devices under consideration. This result directly reflects the significant similarities among the two spectra previously outlined (see Fig. 2).

The comparison between the rates derived from the two approaches (classical and fragmented) can be better evaluated by means of Fig. 10. In the plot, the data are depicted as a function of the LET$_0$ in order to grasp any potential dependency with respect to this parameter. It is noted that, for all the heavy-ion response functions under consideration, the maximum underestimation when using the proposed ion fragmentation method to calculate the space SEL rate is less than a factor of 2, whereas the maximum overestimation is limited to just 30%. Concerning the dependency with respect to the onset LET, it is noted that the largest underestimation occurs toward lower LETs, whereas above 20 MeVcm$^2$/mg, the error is always limited to $\pm$30%. The better agreement for high-LET threshold values is consistent with the fact that, in this particular case, the adjustment between the fragmented and GCR spectra is optimized in the high-LET range. However, other fragmentation combinations and fluence normalizations can be used to improve the agreement in the low and intermediate LET ranges, depending on the specific testing needs and objectives.

## VI. Possible Practical Implementation and Related Limitations

As proposed in this work, using fragmented VHE ion beams can be a useful way of testing electronics for space, thanks to their direct resemblance to the space LET environment, as well as their high penetration capacity. The main challenge linked to its possible implementation and more regular exploitation is, first of all, the limited amount of facilities and beam time availability for VHE ion testing. Currently, only NSRL at BNL [2] and SIS18 at GSI [25] can offer such beams. In the longer run, the CHARM facility at CERN is planned to be used in a similar manner [50], with more energetic (up to 6 GeV/u) heavy ions, and thicker fragmentation targets relative to those used and simulated in this work.

Moreover, putting in place a dosimetry system and procedure to accurately characterize the fragmented beam is also

a significant challenge. Likewise, a thorough experimental benchmark of the obtained results against those retrieved through the classical approach of using the SEE cross section as a function of LET to predict the in-orbit error rate will be needed for a broad range of components and effects, in order to further validate the approach.

Furthermore, some additional key practical aspects for the implementation of this approach are related to the time needed to retrieve a sufficiently large high-LET ($>40$ MeVcm$^2$/mg) fluence on the DUT, as well as the TID levels the parts would receive during the related exposure.

The answer to the first question depends mainly on the level of assurance needed to discard destructive SEEs (e.g., SEL, burnout, gate rupture) for a given mission. Given the fact that this work focuses on the high-LET end of the GCR spectrum, for which the flux in interplanetary space is extremely low ($6.7 \cdot 10^{-8}$ ions/cm$^2$/s, as shown in Section II),we will assume a high-LET ion target fluence of $10^4$ ions/cm$^2$, which, when divided, for instance, by the ten-year high-LET fluence in space yields a factor of almost 500. This fluence of high-LET secondary ions requires in turn, as per the results shown in Section IV, a primary fluence of $2.5 \cdot 10^8$ ions/cm$^2$ which, considering the fluxes available at synchrotron facilities capable of providing such high-energy heavy-ion beams, can be achieved within reasonably short time frames, comfortably in the range of several minutes.

According to the calculations and values shown in Section IV, this fluence would correspond to a TID on the DUT of 40 Gy (or 4 krad), which is typically low enough not to induce cumulative damage and also comparable to the TID a part would receive if tested with various primary ion beams each up to a fluence of $10^7$ ions/cm$^2$, or with 200-MeV protons up to a fluence of $10^{11}$ cm$^{-2}$.

As to what regards the time structure of high-energy ion beams in synchrotron facilities, despite their pulsed nature linked to the acceleration type, beams are obtained through so-called resonant slow extraction [51], with pulses typically lasting hundreds of ms up to several seconds, and with reasonably uniform fluxes during the pulse. The duration of these pulses is orders of magnitude larger than the typical characteristic times for SEEs and, if needed, experimental setups can be synchronized or triggered with the arrival of the pulse. Therefore, flash effects involving multiple ions interacting with the same sensitive element during the same sensitive time window can be excluded. Indeed, as the time between pulses is on the order of several seconds to tens of seconds, the duty cycle is large enough not to have orders of magnitude difference between the flux during a pulse and the average flux.

Otherwise, achieving larger assurance levels, involving high-LET fluences above $10^4$ ions/cm$^2$, is possible by increasing the primary flux and/or exposure time. However, TID issues could emerge, which can qualitatively be attributed to the very large amount of lower LET particles present in the overall spectrum, and which can be seen as an inherent weakness of the approach. Otherwise, a solution for increasing the global fluence without entering dangerous TID regimes would be to test multiple parts, something that can be done in parallel if the beam sizes allow for it, as is typically the case in high-energy heavy-ion facilities (e.g., NSRL at BNL can provide homogeneous beams up to $60 \times 60$ cm).

Moreover, as also shown in Section IV, a significant number of high-energy neutrons is produced in the interaction between the primary high-energy ion beam and the fragmenter. The possible impact of this secondary neutron flux on the device/board under test and its ancillary electronics will also be the topic of future research related to the proposed testing approach. Moreover, the possible SEE impact of surrounding electronics due to light ion fragments emitted with relatively large angles with respect to the primary beam direction will need to be assessed in future work related to this topic. However, as already shown in [11], the mass and LET of secondary fragments decreases very rapidly with emission angle.

Finally, the proposed approach does not deal with angular effects and compares ground-level and space rates assuming mono-directional, normal incidence beams. However, the approach can be generalized to isotropic cases through a combination of experimental and simulation results, knowing that the high penetration capability of the fragmented beam can be exploited to perform tests up to grazing angles.

## VII. Conclusion

We propose an SEE radiation testing approach based on fragmenting high-energy heavy-ion beams in order to obtain a high penetration field closely mimicking parts of the typical LET spectra in space. We introduce the approach in a simplified manner through Monte Carlo simulations in Section II and describe its experimental implementation in Section III, including the related simulations in Section IV, showing a very good agreement with the experimental values, and therefore serving as validation of the fragmented beam characterization and proof-of-principle of the approach. We focus our work on the cosmic LET spectra extending above 40 MeVcm$^2$/mg, that is, beyond the so-called iron knee, however analogous approaches with lighter primary ions can be applied in order to mimic the LET spectrum below 40 MeVcm$^2$/mg. We expect the full LET spectrum in the range of interest for SEEs ($\sim$1–100 MeVcm$^2$/mg) to be reproducible with two single primary ions: one being iron-like, and the second uranium-like.

Thanks to this approach and the very good agreement between the experimental and cosmic LET spectra, SEE rates in space can be directly derived by scaling the experimental rates with the acceleration factor, as is done when using spallation neutrons for atmospheric applications, and as opposed to retrieving SEE rates in space through the convolution of the SEE cross section as a function of LET with the LET spectrum in space. However, the main strength of the approach is rather linked to the highly penetrating nature of the fragmented beam, providing very compatible LET distributions over depths of at least several hundreds of $\mu$m and, therefore, is especially suited for testing devices with complex packages and performing board-level tests.

From a practical implementation point of view, we show that experimental event-by-event energy deposition distribution

results using an 800-MeV/u uranium primary beam at GSI are in very good agreement with Monte Carlo simulations, providing confidence that the latter can be used to accurately describe the mixed and complex nature of the fragmented beam. In addition, we show that the flux of high-LET particles obtained through this approach is large enough to reach the necessary fluences in reasonable time intervals, and that, depending on the secondary high-LET ion fluence target, TID issues can emerge. Moreover, we also performed an initial assessment of the secondary neutron field generated around the fragmenter and potentially affecting ancillary setup elements.

As follow-up steps to the proof-of-concept and fragmented beam characterization validation through measurements and simulations achieved in this work, the approach will need to be further validated through SEE results on different components and including a variety of effects. Future work will also need to incorporate angular effects.

## REFERENCES


[1] J. A. Pellish et al., "Heavy ion testing with iron at 1 GeV/amu," *IEEE Trans. Nucl. Sci.*, vol. 57, no. 5, pp. 2948–2954, Oct. 2010.

[2] C. La Tessa, M. Sivertz, I.-H. Chiang, D. Lowenstein, and A. Rusek, "Overview of the NASA space radiation laboratory," *Life Sci. Space Res.*, vol. 11, pp. 18–23, Nov. 2016.

[3] V. Ferlet-Cavrois et al., "Influence of beam conditions and energy for SEE testing," *IEEE Trans. Nucl. Sci.*, vol. 59, no. 4, pp. 1149–1160, Aug. 2012.

[4] F. Luoni et al., "Beam monitor calibration for radiobiological experiments with scanned high energy heavy ion beams at FAIR," *Frontiers Phys.*, vol. 8, Sep. 2020, Art. no. 568145. [Online]. Available: https://www.frontiersin.org/articles/10.3389/fphy.2020.568145

[5] S. K. Hoeffgen et al., "Investigations of single event effects with heavy ions of energies up to 1.5 GeV/n," *IEEE Trans. Nucl. Sci.*, vol. 59, no. 4, pp. 1161–1166, Aug. 2012.

[6] S. Buchner, N. Kanyogoro, D. Mcmorrow, C. C. Foster, P. M. O'Neill, and K. V. Nguyen, "Variable depth Bragg peak method for single event effects testing," *IEEE Trans. Nucl. Sci.*, vol. 58, no. 6, pp. 2976–2982, Dec. 2011.

[7] P. F. Martinez et al., "SEE tests with ultra energetic Xe ion beam in the CHARM facility at CERN," *IEEE Trans. Nucl. Sci.*, vol. 66, no. 7, pp. 1523–1531, Jul. 2019.

[8] R. G. Alía et al., "Ultraenergetic heavy-ion beams in the CERN accelerator complex for radiation effects testing," *IEEE Trans. Nucl. Sci.*, vol. 66, no. 1, pp. 458–465, Jan. 2019.

[9] M. Kastriotou et al., "Single event effect testing with ultrahigh energy heavy ion beams," *IEEE Trans. Nucl. Sci.*, vol. 67, no. 1, pp. 63–70, Jan. 2020.

[10] A. de Bibikoff and P. Lamberbourg, "Method for system-level testing of COTS electronic board under high-energy heavy ions," *IEEE Trans. Nucl. Sci.*, vol. 67, no. 10, pp. 2179–2187, Oct. 2020.

[11] M. A. Clemens et al., "The effects of nuclear fragmentation models on single event effect prediction," *IEEE Trans. Nucl. Sci.*, vol. 56, no. 6, pp. 3158–3164, Dec. 2009.

[12] R. A. Reed et al., "Impact of ion energy and species on single event effects analysis," *IEEE Trans. Nucl. Sci.*, vol. 54, no. 6, pp. 2312–2321, Dec. 2007.

[13] R. G. Alía et al., "Proton dominance of sub-let threshold GCR see rate," *IEEE Trans. Nucl. Sci.*, vol. 64, no. 1, pp. 388–397, Jan. 2017.

[14] V. Wyrwoll et al., "Heavy ion nuclear reaction impact on SEE testing: From standard to ultra-high energies," *IEEE Trans. Nucl. Sci.*, vol. 67, no. 7, pp. 1590–1598, Jul. 2020.

[15] V. Wyrwoll et al., "Longitudinal direct ionization impact of heavy ions on see testing for ultrahigh energies," *IEEE Trans. Nucl. Sci.*, vol. 67, no. 7, pp. 1530–1539, Jul. 2020.

[16] M. Bagatin et al., "Energy deposition by ultrahigh energy ions in large and small sensitive volumes," *IEEE Trans. Nucl. Sci.*, vol. 69, no. 3, pp. 241–247, Mar. 2022.

[17] C. Ahdida et al., "New capabilities of the FLUKA multi-purpose code," *Frontiers Phys.*, vol. 9, Jan. 2022, Art. no. 788253. [Online]. Available: https://www.frontiersin.org/article/10.3389/fphy.2021.788253

[18] M. H. Mendenhall and R. A. Weller, "A probability-conserving cross-section biasing mechanism for variance reduction in Monte Carlo particle transport calculations," *Nucl. Instrum. Methods Phys. Res. A, Accel., Spectrometers, Detectors Associated Equip.*, vol. 667, pp. 38–43, Mar. 2012.

[19] A. J. Tylka et al., "CREME96: A revision of the cosmic ray effects on micro-electronics code," *IEEE Trans. Nucl. Sci.*, vol. 44, no. 6, pp. 2150–2160, Dec. 1997.

[20] H. Quinn, A. Watkins, L. Dominik, and C. Slayman, "The effect of 1–10-MeV neutrons on the JESD89 test standard," *IEEE Trans. Nucl. Sci.*, vol. 66, no. 1, pp. 140–147, Jan. 2019.

[21] R. G. Alía et al., "Single event effects in high-energy accelerators," *Semicond. Sci. Technol.*, vol. 32, no. 3, Feb. 2017, Art. no. 034003, doi: 10.1088/1361-6641/aa5695.

[22] N. A. Dodds et al., "Hardness assurance for proton direct ionization-induced SEEs using a high-energy proton beam," *IEEE Trans. Nucl. Sci.*, vol. 61, no. 6, pp. 2904–2914, Dec. 2014.

[23] C. C. Foster, P. M. O'Neill, and C. K. Kouba, "Risk assessment based on upset rates from high energy proton tests and Monte Carlo simulations," *IEEE Trans. Nucl. Sci.*, vol. 55, no. 6, pp. 2962–2969, Dec. 2008.

[24] J. C. Chancellor, S. B. Guetersloh, R. S. Blue, K. A. Cengel, J. R. Ford, and H. G. Katzgraber, "Targeted nuclear spallation from moderator block design for a ground-based space radiation analog," 2017, *arXiv:1706.02727*.

[25] C. Schuy, U. Weber, and M. Durante, "Hybrid active-passive space radiation simulation concept for GSI and the future FAIR facility," *Frontiers Phys.*, vol. 8, pp. 337, Aug. 2020. [Online]. Available: https://www.frontiersin.org/article/10.3389/fphy.2020.00337

[26] I. Gordeev and G. Timoshenko, "A new type of ground-based simulator of radiation field inside a spacecraft in deep space," *Life Sci. Sp. Res.*, vol. 30, pp. 66–71, Aug. 2021. [Online]. Available: https://www.sciencedirect.com/science/article/pii/S2214552421000389

[27] C. Cazzaniga et al., "Measurements of ultra-high energy lead ions using silicon and diamond detectors," *Nucl. Instrum. Methods Phys. Res. A, Accel. Spectrom. Detect. Assoc. Equip.*, vol. 985, Jan. 2021, Art. no. 164671.

[28] J. F. Ziegler, M. Ziegler, and J. Biersack, "SRIM—The stopping and range of ions in matter (2010)," *Nucl. Instrum. Methods Phys. Res. Sect. B, Beam Interact. With Mater. Atoms*, vol. 268, no. 11, pp. 1818–1823, 2010. [Online]. Available: https://www.sciencedirect.com/science/article/pii/S0168583X10001862

[29] A. Virtanen, R. Harboe-Sorensen, A. Javanainen, H. Kettunen, H. Koivisto, and I. Riihimaki, "Upgrades for the RADEF facility," in *Proc. IEEE Radiat. Effects Data Workshop*, Jul. 2007, pp. 38–41.

[30] G. Battistoni et al., "Overview of the FLUKA code," *Ann. Nucl. Energy*, vol. 82, pp. 10–18, Aug. 2015.

[31] R. G. Alía, "Radiation fields in high energy accelerators and their impact on single event effects," Ph.D. dissertation, Inst. d'Électronique et des Systèmes, Université de Montpellier, Montpellier, Paris, France, 2013.

[32] V. S. Anashin, A. S. Kuznetsov, A. E. Kozyukov, L. R. Bakirov, A. A. Kazyakin, and K. A. Artemyev, "Compilation of electronic components SEE test results," in *Proc. IEEE Radiat. Effects Data Workshop (REDW)*, Jul. 2013, pp. 30–32.

[33] M. V. O'Bryan et al., "Compendium of current single event effects for candidate spacecraft electronics for NASA," in *Proc. IEEE Radiat. Effects Data Workshop (REDW)*, Jul. 2015, pp. 22–29.

[34] S. Uznanski et al., "SEE and TID test results of candidate electronics for LHC power converter control," in *Proc. IEEE Radiat. Effects Data Workshop (REDW)*, Jul. 2013, pp. 40–44.

[35] V. S. Anashin et al., "SEE test results of electronic components performed on roscosmos test facilities," in *Proc. IEEE Radiat. Effects Data Workshop (REDW)*, Jul. 2014, pp. 205–208.

[36] G. V. Chukov et al., "SEE testing results for RF and microwave ICs," in *Proc. IEEE Radiat. Effects Data Workshop (REDW)*, Jul. 2014, pp. 209–211.

[37] G. R. Allen et al., "2015 compendium of recent test results of single event effects conducted by the jet propulsion Laboratory's radiation effects group," in *Proc. IEEE Radiat. Effects Data Workshop (REDW)*, Jul. 2015, pp. 54–66.

[38] M. V. O'Bryan et al., "Compendium of current single event effects for candidate spacecraft electronics for NASA," in *Proc. IEEE REDW*. Boston, MA, USA, Jul. 2015, pp. 45–53.

[39] F. Irom, S. Vartanian, and G. R. Allen, "Single-event latchup measurements on wireless and powerline network communication devices for use in Mars missions," in *Proc. IEEE Nucl. Space Radiat. Effects Conf. (NSREC)*, Jul. 2018, pp. 1–6.

[40] S. C. Davis, D. J. Mabry, R. Koga, and J. S. George, "SEE and TID testing of components for the near infrared airglow camera (NIRAC)," in *Proc. IEEE Nucl. Space Radiat. Effects Conf. (NSREC)*, Jul. 2018, pp. 39–43.

[41] A. C. Daniel and G. R. Allen, "Heavy-ion test results of several commercial components for use in a class d interplanetary mission payload," in *Proc. IEEE Nucl. Space Radiat. Effects Conf. (NSREC)*, Jul. 2018, pp. 58–62.

[42] F. Bezerra, Personal communication. Paris, Ile-de-France: CNES, May 2018.

[43] C. Virmontois et al., "Dose and single-event effects on a color CMOS camera for space exploration," *IEEE Trans. Nucl. Sci.*, vol. 66, no. 1, pp. 104–110, Jan. 2019.

[44] A. C. Daniel, S. Vartanian, and G. R. Allen, "Radiation effects characterization of commercial multi-channel digital to analog converters for spaceflight applications," in *Proc. IEEE Radiat. Effects Data Workshop*, Jul. 2019, pp. 54–57.

[45] C. H. Pham, D. F. Caughran, and J. J. Likar, "Compendium of recent radiation test results from the Johns Hopkins University applied physics laboratory," in *Proc. IEEE Radiat. Effects Data Workshop*, Jul. 2019, pp. 127–134.

[46] S. C. Davis et al., "The Aerospace Corporation's compendium of recent single event effect results," in *Proc. IEEE Radiat. Effects Data Workshop*, Jul. 2019, pp. 141–148.

[47] J. Budroweit, M. Jaksch, R. G. Alía, A. Coronetti, and A. Kölpin, "Heavy ion induced single event effects characterization on an RF-agile transceiver for flexible multi-band radio systems in NewSpace avionics," *Aerospace*, vol. 7, no. 2, p. 14, Feb. 2020.

[48] S. Vartanian, F. Irom, G. R. Allen, W. P. Parker, and M. D. O'Connor, "Single event latchup results for COTS devices used on SmallSat missions," in *Proc. IEEE Radiat. Effects Data Workshop (Conjunct With NSREC)*, Nov. 2020, pp. 78–81.

[49] R. Ladbury, M. Bay, and J. Zinchuk, "Threats to resiliency of redundant systems due to destructive SEEs," *IEEE Trans. Nucl. Sci.*, vol. 68, no. 5, pp. 970–979, May 2021.

[50] M. Fraser et al., "Feasibility of slow-extracted high-energy ions from the CERN proton synchrotron for CHARM," in *Proc. 13th Int. Particle Accelerator Conf. (IPAC)*. Bangkok, Thailand, Jun. 2022, pp. 1703–1706.

[51] P. A. Sota, P. Burrows, H. Damerau, M. Fraser, M. Vadai, and F. Velotti, "Implementation of RF channeling at the CERN PS for spill quality improvements," in *Proc. 13th Int. Particle Accelerator Conf. (IPAC)*. Bangkok, Thailand, Jun. 2022, pp. 2114–2117.